# The Conformation of NADH Bound to Inosine 5′-Monophosphate Dehydrogenase Determined by Transferred Nuclear Overhauser Effect Spectroscopy†

Céline Schalk-Hihi, Yu-Zhu Zhang, and George D. Markham*

*Institute for Cancer Research, Fox Chase Cancer Center, 7701 Burholme Avenue, Philadelphia, Pennsylvania 19111*

*Received January 28, 1998; Revised Manuscript Received March 23, 1998*

ABSTRACT: Inosine 5′-monophosphate dehydrogenase (IMPDH) catalyzes the oxidation of inosine 5-monophosphate (IMP) to xanthosine 5′-monophosphate (XMP). The reaction proceeds with concomitant conversion of $NAD^+$ to NADH and is the rate-limiting step in the de novo biosynthesis of guanosine nucleotides. IMPDH is a target for numerous chemotherapeutic agents. The conformations of enzyme-bound substrates, enzyme-bound products and enzyme-bound ligands in general, are of interest for the understanding of the catalytic mechanism of the enzyme and the design of new inhibitors. Although several of the chemotherapeutic inhibitors of IMPDH are $NAD^+$ or NADH analogues, no structural data for IMPDH-bound $NAD^+$ (or NADH) are available. In the present work, we have used transferred nuclear Overhauser effect spectroscopy (TRNOESY) to determine the conformation of NADH bound to the active site of human type II IMPDH (IMPDH-h2). The inter-proton distances determined from TRNOESY data indicate that NADH binds to the enzyme active site in an overall extended conformation. The adenosine moiety and the nicotinamide riboside moiety are both in the anti conformation about the glycosidic bond, and both ribose rings are in approximately $C_{4'}$-exo conformations. The nicotinamide amide group was found to be in a cis conformation. The anti conformation of the nicotinamide riboside moiety is in accord with the preferred conformations of several potent and selective dinucleotide inhibitors and is consistent with that implied by the stereospecificity of hydride transfer in the enzymatic reaction. The implications of this conformation for the catalytic mechanism of IMPDH-h2 are discussed.

Inosine 5′-monophosphate dehydrogenase (IMPDH)[1] catalyzes the oxidation of inosine 5′-monophosphate (IMP) to xanthosine 5′-monophosphate (XMP). The reaction is $NAD^+$-dependent and is the rate-limiting step in the de novo biosynthesis of guanosine nucleotides (*1*). Two isoforms of human IMPDH, sharing 84% sequence identity and designated as type I and type II (IMPDH-h1 and IMPDH-h2, respectively), have been isolated (*2, 3*). IMPDH-h2 expression has long been known to be up-regulated in rapidly proliferating human leukemia cell lines, solid tumor tissues, and other cell types, suggesting that IMPDH was a target for isozyme selective inhibitors (*4*−*6*). More recently, it was found that the activity of IMPDH-h1 is also increased in activated lymphocytes, indicating that this isozyme is also an important target for immunosuppressive chemotherapy (*7*).

The catalytic mechanism of IMPDH from various sources has been extensively studied. The kinetic mechanisms initially were found to follow an ordered Bi−Bi pathway with IMP binding before $NAD^+$, and NADH being released before XMP (*8*−*11*). This mechanism differs from the mechanism of most other known $NAD^+$-dependent dehydrogenases in which the binding is either random or $NAD^+$ binds before the substrate (*12*). However, more recent studies have demonstrated a random component to the substrate binding (*13, 14*). IMPDH is one of a group of enzymes that require a monovalent cation, such as $K^+$, for activity (*15*). Recently, the kinetic mechanism for IMPDH-h2 was extended by including the monovalent cation, showing that in the primary kinetic pathway, $K^+$ binds before either substrate (*14*).

The crystal structure of IMPDH from Chinese hamster in a complex formed from IMP and the inhibitor mycophenolic acid (MPA) has been determined by X-ray diffraction (*16*). MPA, an uncompetitive inhibitor of IMPDH with antitumor and immunosuppressive activities, was found bound at the presumed nicotinamide portion of the $NAD^+$ binding site. A covalent bond was seen between the carbon-2 of oxidized IMP and the sulfur atom of Cys-331, suggesting an important

† This work was supported by National Institutes of Health Grants GM51481, GM31186, CA06927; it also was supported by an appropriation from the Commonwealth of Pennsylvania. C.S.-H. and Y.-Z.Z. are recipients of a National Institutes of Health Fellowship Training Grant CA09035. The contents of this manuscript are solely the responsibility of the authors and do not necessarily represent the official views of the National Cancer Institute, or any other sponsoring organization.

* Author to whom correspondence should be addressed. Tel.: 215-728-2439. Fax: 215-728-3574. E-mail: GD_Markham@fccc.edu.

[1] Abbreviations: IMPDH, inosine 5′-monophosphate dehydrogenase; IMPDH-h2, human type II inosine 5′-monophosphate dehydrogenase isozyme; IMP, inosine 5′-monophosphate; XMP, xanthosine 5′-monophosphate; NOE, nuclear Overhauser effect; TRNOE, transferred nuclear Overhauser effect; TRNOESY, transferred nuclear Overhauser effect spectroscopy; FID, free induction decay; TPPI, time-proportional phase incrementation; NAD, β-nicotinamide adenine dinucleotide; NADH, β-nicotinamide adenine dinucleotide reduced form; MPA, mycophenolic acid; TAD, thiazole-4-carboxamide adenine dinucleotide; SAD, selenazole-4-carboxamide adenine dinucleotide. The numbering of the various atoms discussed in this paper is shown in Figure 1. Subscripts N and A denote the nicotinamide riboside moiety and the adenosine moiety, respectively.

S0006-2960(98)00214-1 CCC: $15.00 
Published on Web 04/29/1998

role for this residue in the catalytic mechanism of the enzyme. The crystal structure of IMPDH from the parasite *Tritrichomonas foetus* has recently been determined both as a free enzyme and a noncovalent enzyme·XMP complex (*17*). However, no structural information is available for any IMPDH regarding $NAD^+$ or NADH conformations or interactions. Further insights into the conformations of enzyme-bound ligands will clearly aid in understanding both catalysis and the specificity of IMPDH selective inhibitors. The conformation of bound $NAD^+$(H) is of particular interest since the active metabolite of the antineoplastic agent tiazofurin is a dinucleotide $NAD^+$ analogue (thiazole-adenine dinucleotide, TAD) which has remarkable selectivity for IMPDH over other dehydrogenases for reasons which have not been experimentally explained (*18*−*26*).

Two-dimensional transferred nuclear Overhauser effect spectroscopy (TRNOESY) has recently been used to determine the conformation of a number of flexible small ligand molecules bound at the active sites of macromolecules (*27*−*37*). A combination of the TRNOESY method and molecular modeling showed that IMP bound to the active site of IMPDH-h2 adopts an anti conformation for the glycosyl bond and a C2′-endo pucker conformation for the sugar ring (*38*). This study describes the conformation of NADH bound to IMPDH-h2, as determined by the TRNOESY method. We show that both the adenosine portion and the nicotinamide-riboside portion of NADH adopt anti conformations about their respective glycosidic bonds and provide information on the conformations of the sugar rings and the carboxamide group. These conformational data provide insight into the structural basis for catalysis by IMPDH-h2, and by IMPDHs in general.

## EXPERIMENTAL PROCEDURES

*Preparation of Human IMPDH Type II.* Human IMPDH type II was purified using the procedure described elsewhere (*14*) and exchanged into perdeuterated NMR buffer (20 mM Tris-$d_{11}$, 1 mM dithiothreitol-$d_{10}$, 2% glycerol-$d_8$, 20 mM KCl, pD 8.1 in 99.99% $D_2O$) by running the protein sample through a PD10 column (Pharmacia) preequilibrated with 10 volumes of NMR buffer. The protein was then concentrated in an Amicon pressure cell using a PM10 membrane to a final concentration of 7.66 mg/mL (0.034 mM tetramer, 0.13 mM active sites). Protein concentration was determined from absorbance at 280 nm using an extinction coefficient of 0.465 mg $mL^{-1}$ $cm^{-1}$ and a tetramer molecular weight of 223 kDa (*14*).

NADH (Boehringer Mannheim) and XMP (Sigma) used in the TRNOE experiments were subjected to three cycles of lyophilization and redissolution in 99.9% $D_2O$, using a Speed Vac device (Savant Inc.). A volume of 500 $\mu$L of perdeuterated NMR buffer, containing 0.034 mM IMPDH, was used for the last redissolution to give the required final concentrations of IMPDH, NADH, and XMP, typically 5 mM NADH and 0.5 mM XMP. The [NADH]/[NADH-binding site] ratio was 37, based on previous studies showing that IMPDH contains four binding sites per molecule (*14*). Under these conditions the dissociation constant for NADH was determined to be 0.06 ± 0.01 mM. NMR samples in $H_2O$ were prepared identically except that the solvent was 95% $H_2O$, 5% $D_2O$.

*NMR Spectroscopy.* NMR spectra were recorded at 10 °C on a Bruker DMX600 NMR spectrometer. Two-dimensional TRNOESY spectra were collected with a spectral width of 10 ppm in both dimensions. Six data sets were collected with mixing times of 40, 70, 100, 130, 160, and 200 ms over a period of 60 h. For each spectrum, 500 FIDs were recorded in TPPI mode after 64 dummy scans. For each FID, 1024 complex data points were acquired and 32 scans were accumulated. A relaxation delay of 2 s between each scan was applied. WATERGATE was used to suppress the water peak (*39*−*41*). The IMPDH activity was measured at the end of the experiments, and the enzyme was found to be fully active.

The NMR data were processed on an Indigo II Silicon Graphics computer with the NMR software program FELIX 95 (MSI, Inc.). A $\pi/2$-shifted sine-bell function was applied in each dimension before Fourier transformation, and the $t_1$ dimension was zero-filled to yield a final 1024 × 1024 matrix. The program FACELIFT (National NMR Facility in Madison, WI) was applied to the transformed matrix in order to perform base plane correction (*42*). Initially, the cross-peaks in the 4−5 ppm region of the spectrum, which includes the ribose protons $H_A2'$, $H_A3'$, $H_A4'$, $H_A(5', 5'')$, $H_N2'$, $H_N3'$, $H_N4'$, and $H_N(5', 5'')$ were poorly resolved and difficult to interpret. To improve the spectral resolution in this region, and thus facilitate integration to determine the cross-peak volumes, a digital resolution enhancement procedure was applied. The initial data were zero-filled to 16K complex data points in the $t_2$ dimension and Fourier transformed in this dimension only. A 2K data point segment of the F2 dimension, which included the 3.75 to 5.63 ppm region, was extracted in order to conserve disk space. The data in the $t_1$ dimension were then zero-filled to 32K data points and Fourier transformed. The 3.75 to 6.77 ppm spectral region, which contained 4K data points encompassing the reference $H_N5$-$H_N6$ cross-peak, was extracted. The digital resolution of the resultant spectrum of 2.7 points/Hz in both dimensions was 16 times that of the original spectrum. In addition, a 20° shifted sine bell function was applied to both dimensions before Fourier transformation in order to enhance resolution. Cross-peaks between the adenine ribose protons $H_A1'$, $H_A2'$, $H_A3'$, $H_A4'$, and $H_A(5', 5'')$ and of the proton pairs ($H_N1'$-$H_N3'$) and ($H_N1'$-$H_N4'$) were then well-resolved.

Resonance peaks were assigned based on published spectra of NADH (*43*, *44*). Nuclear Overhauser effect (NOE) cross-peak volumes were integrated and fitted as a function of mixing times to the NOE build-up equation using the program Felix. The initial slopes of the build-up curves gave direct measurements of the cross-relaxation rates between individual proton pairs. The distance between $H_N5$ and $H_N6$ ($r_{H_N5-H_N6}$) which is fixed (2.48 Å) and independent of conformation (*45*) was used as an internal reference to calculate the inter-nuclear distances between individual protons. This proton pair was present in the initial spectrum as well as in the resolution enhanced spectrum and could therefore be used to scale the inter-proton distances obtained from the data processed in both fashions. The cross-relaxation rate between a pair of protons A and B ($R_{A-B}$) was, therefore, compared to the cross-relaxation rate of the $H_N5$-$H_N6$ proton pair ($R_{H_N5-H_N6}$) and the inter-nuclear distance between protons A and B ($r_{A-B}$) was calculated using eq 1.

$$r_{A-B} = r_{H_N5-H_N6}(R_{H_N5-H_N6}/R_{A-B})^{1/6} \quad (1)$$

The NOE-derived inter-nuclear distances were then used to determine the conformation of enzyme-bound NADH. When cross-relaxation rates were available from the initial spectrum as well as from the resolution-enhanced spectrum, the inter-proton distances used to determine the NADH conformation were calculated from the resolution-enhanced spectrum because peak positions were more precise and therefore more reliable. In other cases, the inter-nuclear distances calculated from the initial spectrum were used.

*Model Building and Energy Minimization.* To obtain an energetically favorable structure that was consistent with the NMR data, we generated a computer model of NADH. The adenosine and dihydronicotinamide riboside moieties of NADH were analyzed separately since no cross-peaks between the two moieties were observed. NMR data showed clear cross-relaxation peaks between the adenosine proton $H_A8$ and the ribose protons ($H_A1'$, $H_A2'$, $H_A3'$, $H_A4'$, and $H_A(5', 5'')$), whereas proton $H_A2$ shows a cross-peak with the ribose proton $H_A1'$ only. The adenine ring was thus manually rotated about the glycosidic bond in order to find the best fit between NOE-derived and model-derived inter-proton distances. A constrained energy minimization protocol was then carried out using the program MacroModel (version 5.5, Department of Chemistry, Columbia University), with the AMBER force field. The inter-proton distances determined from the TRNOE experiment were used as constraints allowing a 10% uncertainty in distances without energy penalty. This protocol implicitly ignores magnetization transfer to protein protons which is unobservable in this system. The in vacuo energy-minimized model was then carefully checked to ensure that it still obeyed the NMR distance constraints. For the dihydronicotinamide part of NADH, where the approximate conformation was not initially very clear, a Monte Carlo conformational search with MacroModel was carried out first. In the conformational search procedure, the dihydronicotinamide glycosidic bond was set to be a rotateable bond. The other dihedral angles were not varied during the search. The search was repeated with two different starting geometries about the glycosidic bond (syn and anti) to test for invariance of results. All the individual conformations found were then evaluated by comparison of inter-nuclear distances with the experimentally determined distance constraints to find the conformation which best agreed with the NMR data. Of the 22 and 17 model structures found for the two starting geometries (syn and anti, respectively), none was fully satisfactory. The structure which best obeyed the NMR constraints was modified interactively, by manually rotating about the covalent bonds $H_N2$-$C_N2$-$N_N1$-$C_N6$, $H_N6$-$C_N6$-$N_N1$-$C_N2$ and $H_N1'$-$C_N1'$-$N_N1$-$C_N2$, to satisfy one distance constraint at a time. The inter-nuclear distances measured from the resulting structure were within a 25% error range of the NOE-derived distances. The structure was then energy-minimized using the inter-proton distances from the NOESY measurements as constraints, allowing a 10% uncertainty in distances, to remove energetically unfavorable steric interactions. The minimization was again done using the program MacroModel and the AMBER force field. To get a better fit to the NOE-derived inter-proton distances, the energy-minimized model was then refined by a slight rotation (20°) about the glycosyl bond. No attempts were made to further energy refine the structure since enzymes generally do not bind the lowest energy form of a substrate and the energy of the conformations depends on the force field parameters (*46*, *47*).

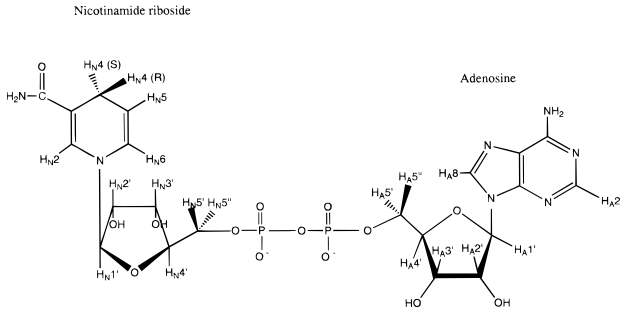


FIGURE 1: Schematic representation and numbering system of NADH.

## RESULTS AND DISCUSSION

*1D $^1$H Spectrum of NADH and Chemical Shift Assignments.* The numbering of the various NADH protons discussed in this work is shown in Figure 1. The $^1$H resonances in the one-dimensional NMR spectrum of NADH, in 10-fold excess with respect to XMP, were assigned based on previously published chemical shifts for NADH (*43*, *44*). Proton chemical shifts for NADH were not affected by the presence of IMPDH and XMP. Weak resonances were seen for the XMP protons since this ligand was used at a low concentration. The presence of XMP was important to ensure the binding of NADH to the active site of the enzyme, since previous studies noted that the E·XMP·NADH complex forms in an ordered fashion with XMP binding first (*13*, *14*). In the one-dimensional NMR spectrum, protons $H_A8$, $H_A2$, $H_N2$, $H_A1'$, and $H_N6$ are well-resolved and have chemical shifts of 8.53, 8.29, 7.00, 6.20, and 6.04 ppm, respectively. Protons $H_N5$ and $H_N1'$ have chemical shifts of 4.80 and 4.85 ppm, respectively. Triplets were obtained for $H_A2'$ and $H_A3'$ at 4.76 and 4.56 ppm, respectively. $H_A4'$ was an isolated multiplet at 4.42 ppm. Protons $H_A(5', 5'')$, $H_N3'$, $H_N2'$, $H_N4'$, and $H_N(5', 5'')$ give multiple peaks between 4.34 and 4.10 ppm which are quite overlapped. However, in the two-dimensional experiments, clearly resolved cross-peaks to the adjacent protons were obtained (see below). The peaks at 2.86 and 2.74 ppm correspond to the diasterotopic dihydropyridine $H_N4$ protons, pro-R and pro-S, respectively. A one-dimensional $^1$H spectrum of the reduced form of $\beta$-nicotinamide mononucleotide ($\beta$-NMNH) confirmed the assignments of the one-dimensional $^1$H NADH spectrum.

*Time-Dependent TRNOE.* Millimolar concentrations of NADH are required for good quality TRNOESY spectra. To evaluate the potential effect of nonspecific binding of NADH, the effect of the dinucleotide concentration on the observed intramolecular interproton NOEs was studied (*28*−*30*). TRNOEs measurements as a function of ligand concentration were performed by varying the NADH concentration from 1 to 5 mM in 1 mM increments, while maintaining the [NADH]/[NADH-binding site] ratio constant at 37. Measurements were made at a single mixing time of 100 ms. The overall two-dimensional spectra were superimposable for each data set. Fractional NOEs for the $A_H1'$-$A_H2'$ and $N_H5$-$N_H6$ proton pairs as a function of NADH concentration in the IMPDH·NADH complex indicated that a 5 mM

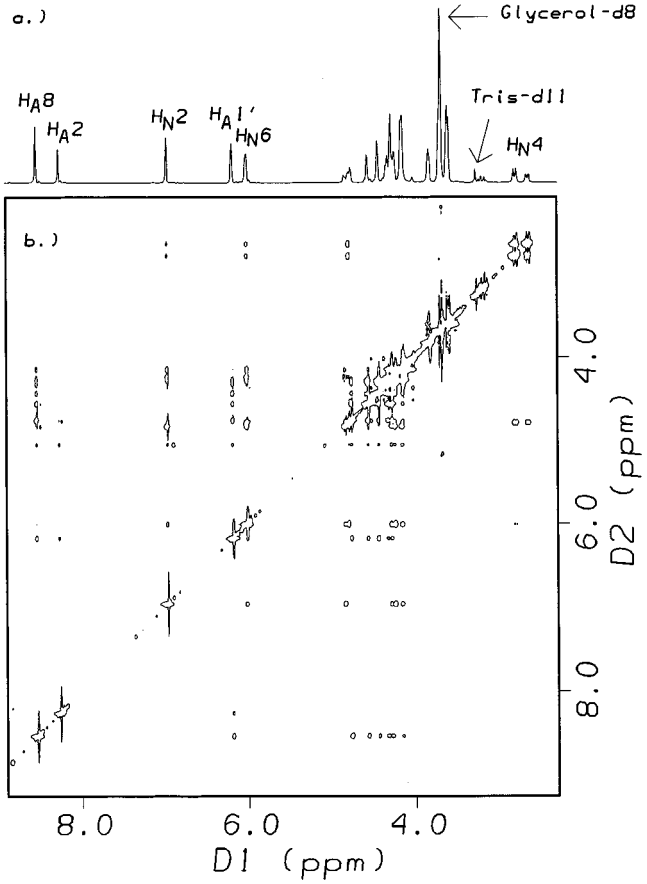


FIGURE 2: (a) One-dimensional $^1$H NMR spectrum of the 0.034 mM IMPDH-h2, 5 mM NADH, 0.5 mM XMP mixture in 99.99% $D_2O$ containing 20 mM Tris-$d_{11}$, 1 mM dithiothreitol-$d_{10}$, 2% glycerol-$d_8$, 20 mM KCl, pD 8.1 at 10 °C; (b) NOESY spectrum of the NADH/XMP/IMPDH-h2 sample described in Figure 2a obtained at 200 ms mixing time.

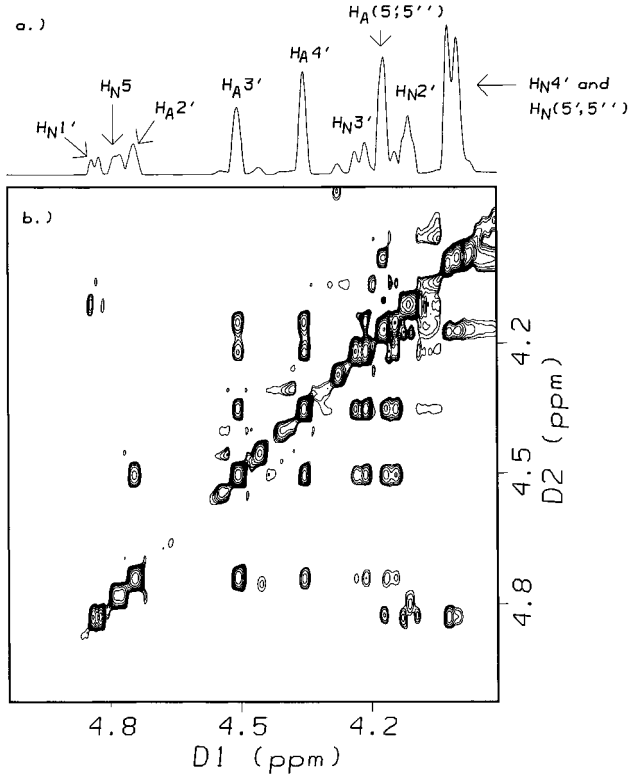


FIGURE 3: Selected portion of the (a) $^1$H NMR spectrum and (b) resolution-enhanced NOESY spectrum showing the ribose region of NADH, of the sample described in Figure 2a, at 200 ms mixing time.

concentration of NADH ensured complete saturation of the active site and no adventitious nucleotide binding. The two-dimensional TRNOESY build-up curves were therefore performed at 5 mM NADH to optimize the signal-to-noise of the data. Figure 2 and Figure 3 show the initial spectrum and the resolution-enhanced spectrum, respectively, at 200 ms mixing time of a sample containing 0.13 mM IMPDH active sites, 5 mM NADH, and 0.5 mM XMP. The $^1$H peaks of the one-dimensional spectrum of NADH are found along the diagonal. For XMP, which was present in the experiment at a low concentration, the diagonal peaks were very weak and are not visible in the figure. The one-dimensional $^1$H spectrum obtained in the same conditions but without protein was used for assignment purposes. No significant difference in the $^1$H chemical shifts between the one-dimensional spectrum and the NOESY spectrum was observed. Off-diagonal cross-peaks were assigned based on the chemical shifts of the diagonal peaks. Cross-peaks primarily reflect cross-relaxation processes in the bound form of NADH since they were not seen in a control experiment, which was performed on a sample containing 5 mM NADH, and 0.5 mM XMP but no IMPDH. The volumes of the NOE cross-peaks from data sets at different mixing times were measured and fitted as a function of their mixing times using the NOE build-up module of the program Felix. These NOE build-up curves were then analyzed to extract inter-proton distances. A direct increase in the cross-peak resonance intensity with increasing mixing time indicated that the distance between the proton pair was less than ~4 Å. The cross-relaxation rate was then measured from the initial slope of the time-dependent NOE build-up curves, and the inter-proton distance was calculated from the cross-relaxation rates using eq 1. For some cross-peaks, a lag phase prior to the time-dependent increase in peak volume was observed which suggested indirect magnetization transfer and indicated that the inter-proton distance was greater than 4 Å. In this case, cross-relaxation rates were not used to calculate an inter-nuclear distance and the distance was assumed to be greater than 4 Å. Typical build-up curves are shown in Figure 4. The inter-proton distances for each proton pair, calculated from the initial slopes of the time-dependent TRNOEs, were then used to determine the conformation of NADH. For proton pairs present in the initial spectrum as well as in the resolution-enhanced spectrum, we used the inter-nuclear distances calculated from the resolution-enhanced spectrum rather than from the initial spectrum, because of their higher accuracy.

The NOE build-up rate of the spatially fixed $H_N5$-$H_N6$ proton pair allows estimation of a 29 ns rotational correlation time for the enzyme·XMP·NADH complex (*28*−*30*). This correlation time is substantially shorter than the value of 120 ns estimated for this 223 kDa protein in 10% glycerol. In a number of studies of ATP utilizing enzymes it has been noted that correlation times deduced from NOESY measurements are significantly shorter than expected based on the protein size; this observation has been attributed to magnetization transfer to the protein protons (*28*−*30*). Fortunately the calculated inter-proton distances, which are based on relative cross relaxation rates within the ligand, are not affected by

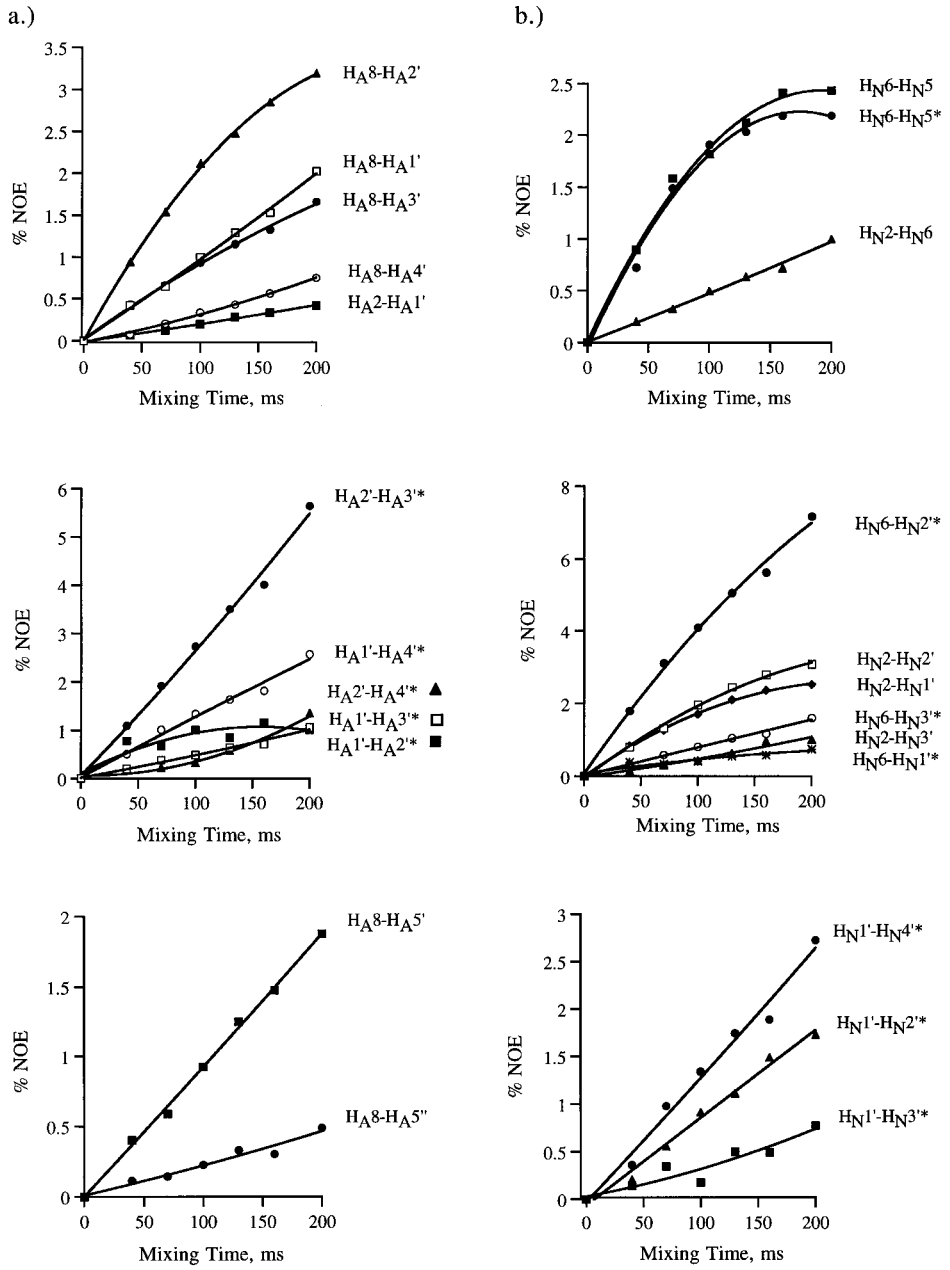


FIGURE 4: NOE intensity build-up curves of the NOE cross-peaks of the (a) adenosine and (b) nicotinamide riboside moiety of different proton pairs of IMPDH-bound NADH. The relative NOE intensity of each proton pair was measured as the ratio of the peak volume at different mixing times to the volume of $H_A3'$ diagonal peak at zero mixing time. The $H_A3'$ diagonal peak is present and well-resolved in the initial spectrum as well as in the resolution-enhanced spectrum. The volume at zero mixing time of the $H_A3'$ diagonal peak was determined by extrapolating the linearly increasing peak volume with decreasing mixing times to zero mixing time. This procedure allowed direct comparison of inter-nuclear distances obtained from the regular spectrum with inter-nuclear distances obtained from the resolution-enhanced spectrum. The * indicates that the NOE percentage was calculated from the resolution-enhanced spectrum.

correlation time, as long as the same correlation time applies to the entire ligand molecule.

*Conformation of NADH. Overall Conformation.* The distance between the adenosine and the nicotinamide ring has been frequently used to describe the overall conformation of NADH. In most of the crystal structures of protein complexes, bound NAD(H) (or NADP(H)) molecules are in some type of open structure with ~15 Å separation between the carbon 6 of the adenine and the carbon 2 of the nicotinamide ring (*48, 49*). In our NMR experiments, no NOEs were seen between the adenosine moiety and the dihydronicotinamide riboside moiety, indicating that NADH bound to IMPDH also adopts a rather extended conformation through the pyrophosphate bridge. However, no additional information concerning the conformation of the pyrophosphate bond could be obtained from the TRNOE data which reflect only local (<4 Å) interactions. Therefore, the conformations of the adenosine and dihydronicotinamide riboside portions of IMPDH-bound NADH were analyzed separately.

*Conformation of the Adenosine Moiety.* Numerous NOE cross-peaks were seen between proton $H_A8$ and the protons in the sugar ring ($H_A1'$, $H_A2'$, $H_A3'$, $H_A4'$, and $H_A(5', 5'')$). In contrast, the $H_A2$ proton showed an NOE cross-peak only with the $H_A1'$ sugar proton. Inter-proton distances calculated from the cross-relaxation rates indicated that proton $H_A8$ is in close proximity to ribose $H_A2'$ (2.51 Å), and slightly further away from proton $H_A3'$ (2.86 Å) and proton $H_A1'$

Table 1: NOE Buildup Parameters of the Adenosine Portion of NADH Bound to IMPDH-h2[a]

| proton pair | $R_{H_N5-H_N6}/R_{A-B}$[b] | $r_{noe}$ (Å) | $r_{em}$ (Å) |
|---|---|---|---|
| $H_A8$-$H_A1'$ | 2.61 | 2.91 | 3.71 |
| $H_A8$-$H_A2'$ | 1.07 | 2.51 | 2.94 |
| $H_A8$-$H_A3'$ | 2.38 | 2.86 | 2.59 |
| $H_A8$-$H_A4'$ | lag phase | >4.0 | 4.43 |
| $H_A8$-$H_A5'$ | 2.72 | 2.93 | 3.26 |
| $H_A8$-$H_A5''$ | 11.39 | 3.72 | 4.18 |
| $H_A2$-$H_A1'$ | 13.40 | 3.82 | 4.42 |
| $H_A1'$-$H_A2'$ | 1.31[c] | 2.59[c] | 2.87 |
| $H_A1'$-$H_A3'$ | 5.53[c] | 3.30[c] | 3.82 |
| $H_A1'$-$H_A4'$ | 1.94[c] | 2.77[c] | 2.95 |
| $H_A2'$-$H_A3'$ | 0.99[c] | 2.47[c] | 2.30 |
| $H_A2'$-$H_A4'$ | lag phase[c] | >4.0[c] | 3.81 |

[a] $R_{A-B}$, cross-relaxation rate between proton A and B; $R_{H_N5-H_N6}$, cross-relaxation rate of the $H_N5$-$H_N6$ proton pair; $r_{noe}$, inter-proton distance determined from the relative NOE intensity referenced to the $H_N5$-$H_N6$ distance of 2.48 Å; and $r_{em}$, inter-proton distance determined from the energy-minimized model. [b] Cross-relaxation rates for the indicated proton pairs are shown as ratios of the rates observed for the $H_N5$-$H_N6$ proton pair to the observed rates of the indicated proton pairs. Cross-relaxation rates were determined from the initial slopes of the NOE build-up curves. [c] Cross-relaxation rates and inter-proton distances calculated from the resolution-enhanced spectrum.

(2.91 Å) (Table 1). The lag phase in the TRNOE build-up curve of the proton pairs $H_A8$-$H_A4'$ (Figure 4a) probably results from the time required to transfer magnetization from $H_A8$ to $H_A4'$ via intermediary spins and indicates that the distance between the two protons is greater than 4 Å. Proton $H_A2$ is 3.82 Å away from $H_A1'$ and more than 4 Å apart from the other ribose protons (data not shown). Taken together, these data indicate that the adenosine moiety of NADH adopts an anti conformation in the active site of IMPDH.

Strong NOE cross-peaks were also observed between proton pairs $H_A1'$-$H_A2'$, $H_A2'$-$H_A3'$, $H_A1'$-$H_A4'$, and $H_A1'$-$H_A3'$. Inter-proton distance calculations from their NOE build-up curves indicated that ribose protons $H_A1'$ and $H_A2'$ are 2.59 Å apart and that $H_A2'$ and $H_A3'$ protons are 2.47 Å apart. The $H_A1'$ proton is in close proximity to the $H_A4'$ proton (2.77 Å) but further from the $H_A3'$ proton (3.30 Å). A lag phase in the build-up curve of the $H_A2'$-$H_A4'$ proton pair indicates indirect magnetization transfer and thus that the two protons are more than 4 Å apart.

The constrained energy-minimized model, based on the inter-proton distances measured from the NOE build-up curves, resulted in a molecule in which, as expected, the adenosine portion of NADH adopts an anti conformation with a torsional angle of the glycosyl bond ($C_A8$-$N_A9$-$C_A1'$-$O_A4'$) of approximately +47°. The sugar ring moiety is in a $C_{4'}$-exo conformation with a pseudorotation phase angle of +65° and a dihedral angle for $C_A1'$-$C_A2'$-$C_A3'$-$C_A4'$ of approximately +19° (Table 2). NMR and crystallographic studies have shown that most characterized protein-bound NAD(H) (or NADP(H)) species adopt anti conformation for the adenosyl glycosidic bond (*48*, *49*). This conformation keeps the $N_A1$-$C_A2$-$N_A3$ portion of the adenosine ring away from the rest of the molecule, making $N_A1$ and $N_A3$ two possible candidates for hydrogen bonds with amino acid residues of the protein ($N_A1$- - -H−E, $N_A3$- - -H−E). The conformation of the sugar ring, while just outside of the classical $C_{3'}$-endo range, moves the $H_A3'$ proton up and close to the $H_A8$ proton. The inter-proton distances of the energy minimized model ($r_{em}$) are very close to the NOE-derived distances ($r_{noe}$) (Table 1). The difference between $r_{noe}$ and $r_{em}$ is generally within a 15% error range. However, this difference is 27% (0.8 Å) for the $H_A8$-$H_A1'$ proton pair, which may indicate that $H_A8$-$H_A1'$ inter-proton NOE-derived distance is overestimated in the energy minimized model. Alternatively the presence of an unobserved protein proton in the vicinity of the $H_A8$-$H_A1'$ vector could lead to underestimation of the NOE derived distance (*50*, *51*). The torsional angles for the ribose in the minimized model are shown in Table 2. The conformation of the adenosine moiety of NADH bound to IMPDH-h2 is illustrated in Figure 5A.

Table 2: Various Torsion Angles and Pseudorotation Phase Angle ($p$) for the Ribose of the Adenosine Portion of the Minimized Model of NADH Bound to IMPDH-h2

| torsion | angle (degree) |
|---|---|
| $\chi$ ($C_A8$-$N_A9$-$C_A1'$-$O_A4'$) | 47 |
| $\nu_0$ ($C_A4'$-$O_A4'$-$C_A1'$-$C_A2'$) | −34 |
| $\nu_1$ ($O_A4'$-$C_A1'$-$C_A2'$-$C_A3'$) | 7 |
| $\nu_2$ ($C_A1'$-$C_A2'$-$C_A3'$-$C_A4'$) | 19 |
| $\nu_3$ ($C_A2'$-$C_A3'$-$C_A4'$-$O_A4'$) | −39 |
| $\nu_4$ ($C_A3'$-$C_A4'$-$O_A4'$-$C_A1'$) | −45 |

$$p = \tan^{-1}\frac{(\nu_4 + \nu_1) - (\nu_3 + \nu_0)}{2\nu_2(\sin 36° + \sin 72°)} = 65$$

*Conformation of the Nicotinamide Riboside Moiety.* The NOE build-up curves shown in Figure 4b indicate that $H_N2$ appears to be in close proximity and nearly equidistant from $H_N1'$ (2.50 Å) and $H_N2'$ (2.48 Å), whereas $H_N6$ is in close proximity to $H_N2'$ (2.24 Å), but much further apart from $H_N1'$ (3.21 Å) (Table 3). The linear increase in the NOE values with mixing time for these four different proton pairs confirms that these distances are reliable. The occurrence of a short lag phase prior to the linear increase in the NOE build-up curve for the proton pair $H_N2$-$H_N3'$ indicates that there is little direct cross-relaxation between these two protons and that the distance measured from the build-up curve probably underestimates the correct distance which thus is greater than ∼4 Å. On the other hand, the time-dependence of the build-up curve of the $H_N6$-$H_N3'$ pair shows a direct increase in the cross-peak volume (without a lag phase) and indicates that these two protons have direct magnetization transfer; a distance of 3.01 Å is calculated. These distances can be achieved only if the conformation of the nicotinamide riboside moiety is in an anti form. The conformational search-derived nicotinamide riboside structure with the glycosyl bond in an anti conformation (see Experimental Procedures) was therefore chosen as a starting model for further analysis. This structure was first refined manually in order to find the best fit between NOE-derived distances and model-derived inter-proton distances. The model was then energy-minimized. The resulting model, which was geometrically close to the starting geometry, was refined further by manually rotating about the glycosyl bond in order to provide the best fit between NOE-derived and model-measured inter-nuclear distances. The final model has an anti orientation about the glycosyl bond with a $C_N2$-$N_N1$-$C_N1'$-$O_N4'$ torsional angle of approximately −170°. The ribose ring is in the $C_{4'}$-exo conformation with pseudorotation phase angle of +52° and a $C_N1'$-$C_N2'$-$C_N3'$-$C_N4'$ dihedral angle of approximately +26° (Table 4). The inter-proton distances between proton pairs in the ribose ring $H_N1'$-$H_N2'$,

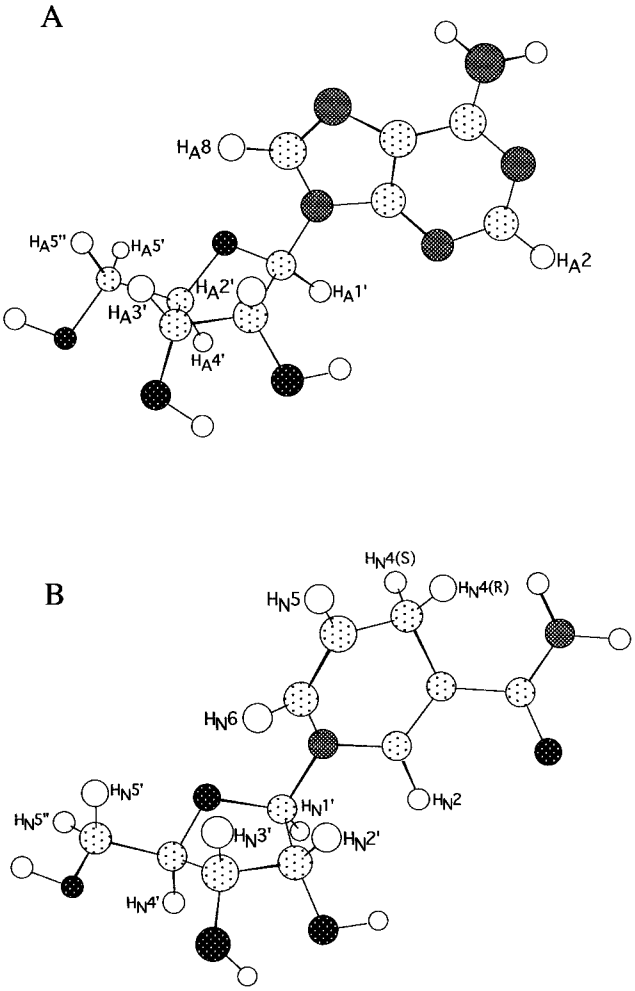


FIGURE 5: Computed conformation of the (A) adenosine moiety and (B) nicotinamide riboside moiety of IMPDH-h2-bound NADH based on the experimental distances in Tables 1 and 3. White, light gray, dark gray, and black circles represent hydrogen, carbon, nitrogen, and oxygen atoms, respectively.

$H_N1'$-$H_N4'$ are 3.02 Å and 2.81 Å, respectively. A lag phase in the build-up curve of the $H_N1'$-$H_N3'$ proton pair indicated that the inter-nuclear distance between these two protons is probably greater than 4.0 Å. The inter-proton distances measured from the final model are within a 20% error range from the inter-proton distances calculated from the time-dependent NOEs (Table 3). The conformation of the nicotinamide riboside moiety of IMPDH-h2-bound-NADH is illustrated in Figure 5B.

To obtain information about the orientation of the carboxamide group with respect to the nicotinamide ring, a NOESY experiment was conducted in 95% $H_2O$, 5% $D_2O$. A broad peak was seen at 7.06 ppm for the amide protons. The NOESY spectra obtained (Figure 6) show clear cross-peaks between the amide proton resonance and the $H_N4$ protons, indicating that the amide group is in a cis conformation, which in solution is energetically more favorable than the trans conformation (*52*). It has been noted that in enzyme-bound $NAD^+$ the carboxamide group is usually slightly out-of-plane with respect to the nicotinamide ring and that the out-of-plane rotation of the carbonyl function controls the stereospecificity of the introduced hydride anion (*53*, *54*). It appears difficult, however, to get detailed structural information regarding the out-of-plane orientation of the carboxamide group from our NOESY experiment since the distance difference between the carboxamide and the $H_N4$ protons is rather small. However, Figure 6B suggests that the carboxamide protons are nearer to the pro-R $H_N4$ proton which would leave the pro-S hydrogen sterically unhindered for reaction.

Table 3: NOE Buildup Parameters of the Nicotinamide Riboside Portion of NADH Bound to IMPDH-h2[a]

| proton pair | $R_{H_N5-H_N6}/R_{A-B}$[b] | $r_{noe}$ (Å) | $r_{em}$ (Å) |
|---|---|---|---|
| $H_N6$-$H_N5$ | 1 | 2.48 | 2.53 |
| | 1[c] | 2.48[c] | |
| $H_N6$-$H_N2$ | 5.36 | 3.28 | 3.84 |
| $H_N6$-$H_N1'$ | 4.71[c] | 3.21[c] | 3.63 |
| $H_N6$-$H_N2'$ | 0.55[c] | 2.24[c] | 2.55 |
| $H_N6$-$H_N3'$ | 3.21[c] | 3.01[c] | 2.34 |
| $H_N2$-$H_N1'$ | 1.05 | 2.50 | 2.48 |
| $H_N2$-$H_N2'$ | 1.01 | 2.48 | 2.68 |
| $H_N2$-$H_N3'$ | lag phase | >4.0 | 4.52 |
| $H_N1'$-$H_N2'$ | 3.25[c] | 3.02[c] | 2.93 |
| $H_N1'$-$H_N3'$ | lag phase[c] | >4.0[c] | 3.75 |
| $H_N1'$-$H_N4'$ | 2.14[c] | 2.81[c] | 2.79 |
| $H_N5$-$H_N4$(pro-R) | 0.99 | 2.48 | 2.45 |
| $H_N5$-$H_N4$(pro-R) | 0.55 | 2.25 | 2.81 |
| $H_N6$-$H_N4$(pro-R) | lag phase | >4.0 | 4.22 |
| $H_N6$-$H_N4$(pro-S) | lag phase | >4.0 | 4.09 |

[a] $R_{A-B}$, cross-relaxation rate between proton A and B; $R_{H_N5-H_N6}$, cross-relaxation rate of the $H_N5$-$H_N6$ proton pair; $r_{noe}$, inter-proton distance determined from the NOE intensity referenced to the $H_N5$-$H_N6$ distance of 2.48 Å; and $r_{em}$, inter-proton distance determined from the energy-minimized model. [b] Cross-relaxation rates for the indicated proton pairs are shown as ratios of the rates observed for the $H_N5$-$H_N6$ proton pair to the observed rates of the indicated proton pairs. Cross-relaxation rates were determined from the initial slopes of the NOE build-up curves. [c] Cross-relaxation rates and inter-proton distances calculated from the resolution-enhanced spectrum.

Table 4: Various Torsion Angles and Pseudorotation Phase Angle ($p$) for the Ribose of the Nicotinamide Ribose Portion of the Minimized Model of NADH Bound to IMPDH-h2

| torsion | angle (degree) |
|---|---|
| $\chi$ ($C_N2$-$N_N1$-$C_N1'$-$O_N4'$) | −170 |
| $\nu_0$ ($C_N4'$-$O_N4'$-$C_N1'$-$C_N2'$) | −23 |
| $\nu_1$($O_N4'$-$C_N1'$-$C_N2'$-$C_N3'$) | −3 |
| $\nu_2$($C_N1'$-$C_N2'$-$C_N3'$-$C_N4'$) | 26 |
| $\nu_3$($C_N2'$-$C_N3'$-$C_N4'$-$O_N4'$) | −41 |
| $\nu_4$($C_N3'$-$C_N4'$-$O_N4'$-$C_N1'$) | 40 |

$$p = \tan^{-1}\frac{(\nu_4 + \nu_1) - (\nu_3 + \nu_0)}{2\nu_2(\sin 36° + \sin 72°)} = 52$$

## CONCLUSION

The NOE-derived data described in the present work indicate that the glycosidic conformations of both nicotinamide-ribose and adenosine moieties are anti. It is useful to place this observation in the context of other NAD(P) using enzymes. Twenty of 22 dehydrogenases and reductases of known crystal structure bind the adenosine group in the anti conformation with glycosidic torsional angles broadly distributed about approximately +70° (*49*). TRNOESY results for mononucleotides bound to several adenosine mononucleotide utilizing enzymes have revealed similar torsional angles about the glycosidic bond (C8-N9-C1′-O4′) of 52° ± 8° (*30*); this range encompasses the value of 47° found in this study for the adenosine moiety of NADH bound to IMPDH and of 57° that was found for IMP bound to IMPDH (*38*). This

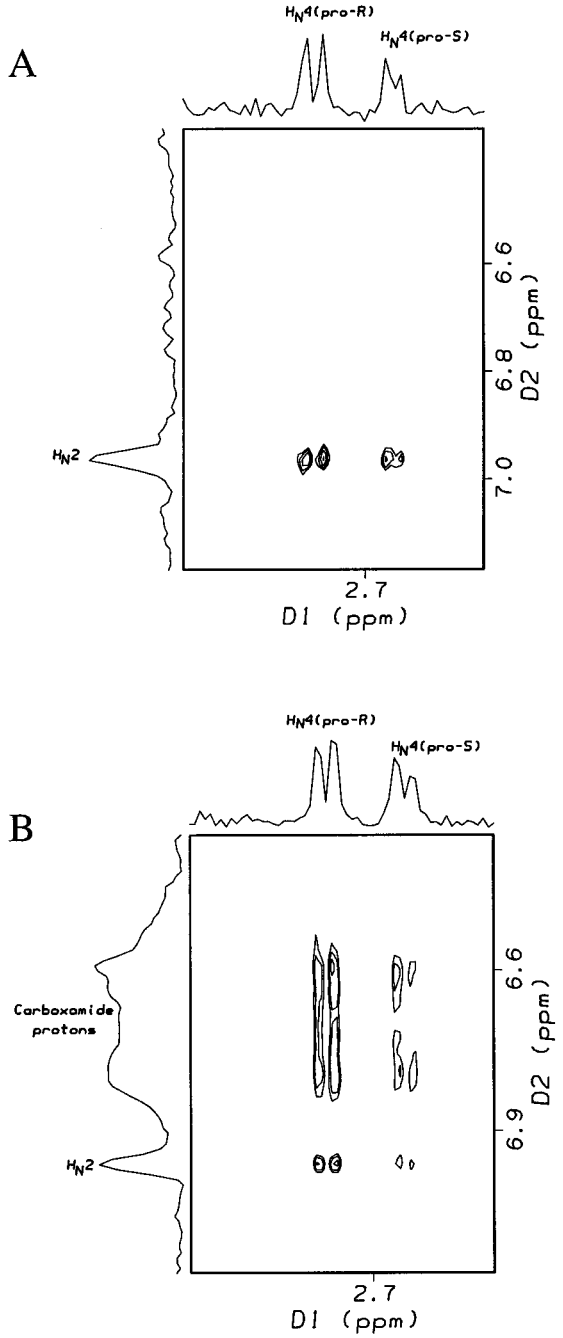


FIGURE 6: Cross-peaks between the carboxamide amide protons and the pro-R and pro-S nicotinamide $H_N4$ protons observed in the spectrum performed in 95% $H_2O$ but not in 99% $D_2O$. Selected portion of the NOESY spectrum of the NADH/XMP/IMPDH-h2 mixture obtained at 200 ms mixing time. Data are from experiments performed in (B) 95% $H_2O$, 5% $D_2O$, and (A) 99.99% $D_2O$. Solutions contained other components as described in the legend for Figure 2.

common geometrical arrangement has been proposed as a structural motif for binding (*30*), and may reflect a preferred conformation for purine nucleotides (*49*). The conformation about the nicotinamide riboside glycosidic bond is more variable ranging from syn to anti (*49*). The torsional angle about the nicotinamide glycosidic bond has been correlated with the stereospecificity of hydride transfer (*48*, *55*). The stereospecificity of IMPDH from several sources, including the present human IMPDH-h2 enzyme, has been studied indicating that IMPDHs are B-type dehydrogenases with hydride transfer occurring to the pro-S side of the $NAD^+$ nicotinamide ring (*56*−*58*). It has been noted that typically B-type dehydrogenases bind the $NAD^+$ cofactor with the nicotinamide-riboside in an anti orientation when $NAD^+$ binds on top of the substrate (*55*). This is consistent both with the observation that IMPDH preferentially binds IMP before $NAD^+$ (*8*−*14*) and with crystallographic studies showing that the product XMP binds at the bottom of a cavity in the protein (*17*, *18*). The precise location of the NAD(H) binding site within the protein remains as yet unclear. Two C-glycosides, TAD and SAD (thiazole- and selenazole-4-carboxamide adenine dinucleotides), potent inhibitors of IMPDH, appear likely to bind to the dinucleotide binding site of IMPDH by adopting an anti orientation about their thiazole (or selenazole) glycosidic bond (*60*−*62*). This orientation is stabilized by an intramolecular electrostatic interaction between the ribose oxygen and the partially positively charged S/Se atoms (*23*, *24*). Modeling studies on MPA, another potent IMPDH inhibitor that binds to the nicotinamide portion of the dinucleotide binding site (*63*), suggested that MPA binds by adopting an anti-like conformation (*64*). Thus it appears that the nicotinamide conformation of IMPDH-bound NADH is related to the unusually high affinity of IMPDH for nicotinamide-substituted analogues such as TAD and SAD which lack the positive charge of the $NAD^+$ nicotinamide ring and thus are best described as NADH analogues rather than $NAD^+$ analogues (*60*−*63*). The present NOE data also indicate that the carboxamide moiety is not coplanar with the nicotinamide ring and lies closer to the $H_N4$ proton that is not involved in hydride transfer (the pro-R proton), thus leaving the pro-S proton sterically unhindered for participation in the reaction. This positioning of the carboxamide group places the carbonyl group syn to the hydrogen involved in the reaction, consistent with studies of model systems (*54*). Thus the conformation of IMPDH-bound NADH determined from the NOE measurements is in excellent accord with that predicted based on mechanistic considerations and rationalizes the characteristics of potent inhibitors.

## ACKNOWLEDGMENT

We thank Dr. Robert Petrovich for helpful discussions and Dr. Hong Cheng for assistance in NMR instrument operation and data processing.

## REFERENCES

1. Jackson, R. C., Weber, G., and Morris, H. P. (1975) *Nature 256*, 331−333.
2. Collart, F. R., and Hubermann, E. (1988) *J. Biol. Chem. 263*, 15769−15772.
3. Natsumeda, Y., Ohno, S., Kawasaki, H., Konno, Y., Weber, G., and Suzuki, K. (1990) *J. Biol. Chem. 265*, 5292−5295.
4. Collart, F. R., Chubb, C. B., Mirkin, B. L., and Huberman, E. (1992) *Cancer Res. 52*, 5826−5828.
5. Konno, Y., Natsumeda, Y., Nagai, M., Yamaji, Y., Ohno, S., Suzuki, K., and Weber, G. (1991) *J. Biol. Chem. 266*, 506−509.
6. Nagai, M., Natsumeda, Y., Konno, Y., Hoffman, R., Irino, S., and Weber, G. (1991) *Cancer Res. 51*, 3886−3890.
7. Dayton, J. S., Linsten, T., Thompson, C. B., and Mitchell, B. S. (1994) *J. Immunol. 152*, 984−991.
8. Jackson, R. C., Morris, H. P., and Weber, G. (1977) *Biochem. J. 166*, 1−10.
9. Carr, S. F., Papp, E., Wu, J. C., and Natsumeda, Y. (1993) *J. Biol. Chem. 268*, 27286−27290.

10. Verham, R., Meek, T. D., Hedstrom, L., and Wang, C. C. (1987) *Mol. Biochem. Parasitol. 24*, 1−12.
11. Hupe, D. J., Azzolina, B. A., and Behrens, N. D. (1986) *J. Biol. Chem. 261*, 8363−8369.
12. Fersht, A. (1984) *Enzyme Structure and Mechanism*, 2nd ed., pp 390−404, W. H. Freeman, New York.
13. Wang, W., and Hedstrom, L. (1997) *Biochemistry 36*, 8479−8483.
14. Xiang, B., Taylor, J. C., and Markham, G. D. (1996) *J. Biol. Chem. 271*, 1435−1440.
15. Suelter, C. H. (1970) *Science 168*, 789−795.
16. Sintchack, M. D., Fleming, M. A., Futer, O., Raybuck, S. A., Chambers, S. P., Caron, P. R., Murcko, M. A., and Wilson, K. P. (1996) *Cell 85*, 921−930.
17. Whitby, F. G., Luecke, H., Kuhn, P., Somoza, J. R., Huete-Perez, J. A., Phillips, J. D., Hill, C. P., Fletterick, R. J., and Wang, C. C. (1997) *Biochemistry 36*, 10666−10674.
18. Cooney, D. A., Jayaram, H. N., Gebeyehu, G., Betts, C. R., Kelley, J. A., Marquez, V. E., and Johns, D. G. (1982) *Biochem. Pharmacol. 31*, 2133−2136.
19. Jayaram, H. N., Dion, R. L., Glazer, R. I., Johns, D. G., Robins, R. K., Srivastava, P. C., and Cooney, D. A. (1982) *Biochem. Pharmacol. 31*, 2371−2380.
20. Goldstein, B. M., Bell, J. E., and Marquez, V. E. (1990) *J. Med. Chem. 33*, 1123−1127.
21. Marquez, V. E., Tseng, C. K. H., Gebeyehu, G., Cooney, D. A., Ahluwalia, G. S., Kelley, J. A., Dalal, M., Fuller, R. W., Wilson, Y. A., and Johns, D. G. (1986) *J. Med. Chem. 29*, 1726−1731.
22. Tricot, G. J., Jayaram, H. N., Lapis, E., Natsumeda, Y., Nichols, C. R., Kneebone, P., Heerema, N., Weber, G., and Hoffman, R. (1989) *Cancer Res. 49*, 3696−3701.
23. Li, H., Hallows, W. H., Punzi, J. S., Marquez, V. E., Carrell, H. L., Pankiewicz, K. W., Watanabe, K. A., and Goldstein, B. M. (1994) *Biochemistry 33*, 23−32.
24. Burling, F. T., and Goldstein, B. M. (1992) *J. Am. Chem. Soc. 114*, 2313−2320.
25. Zatorski, A., Watanabe, K. A., Carr, S. F., Goldstein, B. M., and Pankiewicz, K. W. (1996) *J. Med. Chem. 39*, 2422−2426.
26. Lui, M. S., Faderan, M. A., Liepnieks, J. J., Natsumeda, Y., Olah, E., Jayaram, H. N., and Weber, G. (1984) *J. Biol. Chem. 259*, 5078−5082.
27. Plesniak, L. A., Yu, L., and Dennis, E. A. (1995) *Biochemistry 34*, 4943−4951.
28. Jarori, G. K., Murali, N., and Nageswara Rao, B. D. (1994) *Biochemistry 33*, 6784−6791.
29. Murali, N., Jarori, G. K., Landy, S. B., and Nageswara Rao, B. D. (1993) *Biochemistry 32*, 12941−12948.
30. Murali, N., Lin, Y., Mechulam, Y., Plateau, P., and Nageswara Rao, B. D. (1997) *Biophys. J. 70*, 2275−2284.
31. Song, S., Velde, D. V., Gunn, C. W., and Himes, R. H. (1994) *Biochemistry 33*, 693−698.
32. Stewart, J. M. M., Jorgensen, P. L., and Grisham, C. M. (1989) *Biochemistry 28*, 4695−4701.
33. Rosevear, P. R., Bramson, H. N., O'Brian, C., Kaiser, E. T., and Mildvan, A. S. (1983) *Biochemistry 22*, 3439−3447.
34. Perlman, M. E., Davis, D. G., Koszalka, G. W., Tuttle, J. V., and London, R. E. (1994) *Biochemistry 33*, 7547−7559.
35. Koblan, K. S., Culberson, J. C., Desolms, S. J., Giuliani, E. A., Mosser, S. D., Omer, C. A., Pitzenberger, S. M., and Bogusky, M. J. (1995) *Protein Sci. 4*, 681−688.
36. Ehrlich, R. S., and Colman, R. F. (1990) *Biochemistry 29*, 5179−5187.
37. Seelig, G. F., Prosise, W. W., Hawkins, J. C., and Senior, M. M. (1995) *J. Biol. Chem. 270*, 9241−9249.
38. Xiang, B., and Markham, G. D. (1996) *J. Biol. Chem. 271*, 27531−27535.
39. Piotto, M., Saudek, V., and Sklenár, V. (1992) *J. Biomol. NMR 2*, 661−665.
40. Sklenár, V., Piotto, M., Leppik, R., and Saudek, W. (1993) *J. Magn. Reson. 102*, 241−245.
41. Wang, C., and Pardi, A. (1987) *J. Magn. Reson. 71*, 154−158.
42. Chylla, R. A., and Markley, J. L. (1993) *J. Magn. Reson. 102*, 148−154.
43. Oppenheimer, N. J., Ed. (1982) in *The Pyridine Nucleotide Coenzymes*, pp 51−89, Academic Press, New York.
44. Oppenheimer, N. J. (1987) in *The Pyridine Nucleotide Coenzymes. Chemical, Biochemical, and Medical Aspects* (Dolphin, D., Avramoric, O., and Poulson, R., Eds.) Vol. 2, Part A, Chapter 7, John Wiley and Sons, New York.
45. Clore, G. M., and Gronenborn, A. M. (1983) *J. Magn. Reson. 53*, 423−442.
46. Mildvan, A. S. (1981) *Philos. Trans. R. Soc. London, Ser. B 293*, 65.
47. Rosevear, P. R., and Mildvan, A. S. (1989) *Methods Enzymol. 1977*, 333−358.
48. Eklund, H., and Brädén, C.-I. (1987) in *Pyridine Nucleotide Coenzymes. Chemical, Biochemical, and Medical Aspects* (Dolphin, D., Avramovic, O., and Poulson, R., Eds.), Vol. 2, Part A, Chapter 4, John Wiley and Sons, New York.
49. Bell, C. E., Yeates, T. O., and Eisenberg, D. (1997) *Protein Sci. 6*, 2084−2096.
50. Landy, S. B., and Nageswara Rao, B. D. (1993) *J. Magn. Reson. B102*, 209−213.
51. Moseley, H. N. B., Curto, E. V., and Rama Krishna, N. (1995) *J. Magn. Reson. B108*, 243−261.
52. Wu, Y.-D., Lai, D. K. W., and Houk, K. N. (1995) *J. Am. Chem. Soc. 117*, 4102−4108.
53. Donkersloot, M. C. A., and Buck, H. M. (1981) *J. Am. Chem. Soc. 103*, 6554−6558.
54. de Kok, P. M. T., Donkersloot, M. C. A., van Lier, P. M., Meulendijks, G. H. W. M., Bastiaansen, L. A. M., van Hoof, H. J. G., Kanters, J. A., and Buck, H. M. (1986) *Tetrahedron 42*, 941−959.
55. Oppenheimer, N. J., and Handlon, A. L. (1992) *The Enzymes*, 3rd ed., Vol. 20, pp 454−506, Academic Press, New York.
56. Cooney, D., Hamel, E., Cohen, M., Kang, G. J., Dalal, M., and Marquez, V. (1987) *Biochim. Biophys. Acta 916*, 89−93.
57. You, K. (1985) *Crit. Rev. Biochem. 17*, 313−415.
58. Xiang, B., and Markham, G. D. (1997) *Arch. Biochem. Biophys. 348*, 378−382.
59. Wu, Y. D., and Houk, K. N. (1991) *J. Am. Chem. Soc. 113*, 2353−2358.
60. Gebeyehu, G., Marquez, V. E., Van Cott, A., Cooney, D. A., Kelley, J. A., Jayaram, H. N., Ahluwalia, G. S., Dion, R. L., Wilson, Y. A., and Johns, D. G. (1985) *J. Med. Chem. 28*, 99−105.
61. Yamada, Y., Natsumeda, Y., and Weber, G. (1988) *Biochemistry 27*, 2193−2196.
62. Cooney, D. A., Jayaram, H. N., Glazer, R. I., Keley, J. A., Marquez, V. E., Gebeyehu, G., Van Cott, A. C., Zwelling, L. A., and Johns, D. G. (1983) *Adv. Enzyme Regul. 21*, 271−303.
63. Hedstrom, L., and Wang, C. C. (1990) *Biochemistry 29*, 849−854.
64. Makara, M. G., Keserû, G. M., Kajtár-Peredy, M., and Anderson, W. K. (1996) *J. Med. Chem. 39*, 1236−1242.

BI980214H